The influence of boundary conditions on wall shear stress distribution in patients specific coronary trees

Alina G. van der Giessen [a,e], Harald C. Groen [a], Pierre-André Doriot [f], Pim J. de Feyter [b,c], Antonius F.W. van der Steen [a,d], Frans N. van de Vosse [e], Jolanda J. Wentzel [a], Frank J.H. Gijsen [a,*]

[a] Department of Biomedical Engineering, Erasmus Erasmus MC, Biomechanics Laboratory Ee2322, PO Box 2040, 3000 CA Rotterdam, The Netherlands
[b] Department of Cardiology, Erasmus MC, Rotterdam, The Netherlands
[c] Department of Radiology, Erasmus MC, Rotterdam, The Netherlands
[d] The Interuniversity Cardiology Institute of the Netherlands, Utrecht, The Netherlands
[e] Department of Biomedical Engineering, University of Technology Eindhoven, Eindhoven, The Netherlands
[f] Cardiology Division, University Hospital, Geneva, Switzerland

ARTICLE INFO

ABSTRACT

Patient specific geometrical data on human coronary arteries can be reliably obtained multislice computer tomography (MSCT) imaging. MSCT cannot provide hemodynamic variables, and the outflow through the side branches must be estimated. The impact of two different models to determine flow through the side branches on the wall shear stress (WSS) distribution in patient specific geometries is evaluated.

Murray's law predicts that the flow ratio through the side branches scales with the ratio of the diameter of the side branches to the third power. The empirical model is based on flow measurements performed by Doriot et al. (2000) in angiographically normal coronary arteries. The fit based on these measurements showed that the flow ratio through the side branches can best be described with a power of 2.27. The experimental data imply that Murray's law underestimates the flow through the side branches.

We applied the two models to study the WSS distribution in 6 coronary artery trees. Under steady flow conditions, the average WSS between the side branches differed significantly for the two models: the average WSS was 8% higher for Murray's law and the relative difference ranged from −5% to +27%. These differences scale with the difference in flow rate. Near the bifurcations, the differences in WSS were more pronounced: the size of the low WSS regions was significantly larger when applying the empirical model (13%), ranging from −12% to +68%.

Predicting outflow based on Murray's law underestimates the flow through the side branches. Especially near side branches, the regions where atherosclerotic plaques preferentially develop, the differences are significant and application of Murray's law underestimates the size of the low WSS region.

© 2011 Elsevier Ltd. Open access under the Elsevier OA license.

1. Introduction

Flow induced wall shear stress (WSS) is an important parameter in the localization of early atherosclerosis. It has been demonstrated that sites with low WSS, including regions close to bifurcations are more atherogenic (Malek et al., 1999; Cunningham and Gotlieb, 2005; Jeremias et al., 2000). The influence of WSS on the progression of atherosclerosis in the more advanced stages of the disease is largely unresolved and in vivo studies are required to study this topic further (Wentzel et al., 2003; Slager et al., 2005; Chatzizisis et al., 2008).

Computational fluid dynamics (CFD) is a frequently applied technique to assess time-averaged WSS distribution in human coronary arteries. This technique requires information on the 3D geometry of the artery, preferably combined with hemodynamic data, which need to be prescribed as boundary conditions at the inlet of the artery and at the outlet of the side-branches. To obtain 3D coronary geometries and hemodynamic data most studies rely on invasive catheter based imaging techniques, such as intravascular ultrasound (IVUS) (Chatzizisis et al., 2008; Slager et al., 2000). The application of these techniques to assess the geometry in and around coronary bifurcation regions is laborious (Gijsen

et al., 2007) and less suitable for repeated WSS assessment over time because of their invasive nature.

Multislice computed tomography (MSCT) coronary angiography is a promising imaging technique capable of visualizing the coronary artery non-invasively. Although temporal and spatial resolution of the currently available MSCT equipment cannot match invasive technologies, MSCT is the best among non-invasive imaging techniques and radiation dose is now within limits such that serial imaging over time is acceptable. We expect that further developments in the near future result in increased resolutions such that 3D lumen reconstruction will be accurate enough for WSS computations. Since MSCT can image both the main branch and the side branches, it provides the geometrical data required to compute WSS near bifurcations. However, MSCT cannot provide the flow at the inlet or through the side branches.

Studies on WSS patterns in human coronary arteries are regularly performed without patient-derived flow measurements (Krams et al., 1997; Frauenfelder et al., 2007; Soulis et al., 2006). To determine the inflow, these studies assume an average WSS at the inlet or a Reynolds number typical for coronary artery flow (Joshi et al., 2004; Perktold et al., 1991; He and Ku 1996), leading to a wide variety of average WSS values. For the flow through the side branches, some studies that computed time-averaged WSS in coronary geometries prescribed stress-free outflow in the side-branches (Boutsianis et al., 2004). Other studies assume that the average WSS in the mother branch upstream of a bifurcation is equal to the average WSS in both the daughter branches downstream of a bifurcation (LaBarbera, 1990). Combined with Poiseuille's law, the flow ratio through the side branches can be estimated

$$\frac{q_{D2}}{q_{D1}} = \left(\frac{d_{D2}}{d_{D1}}\right)^3 \tag{1}$$

with q_{D1} and q_{D2} the flow through and d_{D1} and d_{D2} the diameters of the branches. This relationship is also known as Murray's Law, and although one can assume that it predicts more realistic flow distributions than stress-free outlet conditions, it is debatable

how well this law applies to healthy and diseased coronary arteries. Studies that modeled the coronary tree geometry and related flow and diameter, report different, and constantly lower, power values than the cubed power from Murray's Law (VanBavel and Spaan 1992; Mittal et al., 2005; Huo and Kassab, 2007).

The combination of diameter and flow measurements in human coronary arteries in both mother and side-branches has only been reported once by Doriot et al. (2000). In the current study, we use these measurements to establish the relation between flow and diameter, and diameter ratio and flow ratio. These relationships were used to determine inflow and outflow boundary conditions for CFD simulations. We will demonstrate the impact of prescribing these boundary conditions versus boundary conditions obtained from Murray's Law on the WSS distribution in patient-specific coronary bifurcations.

2. Methods

2.1. Flow–diameter relation

In order to derive the flow–diameter relation for the inflow and the flow ratio in the bifurcations we used the measurements of Doriot et al. (2000). In 21 patients that underwent cardiac catheterization for various cardiac diseases, intracoronary Doppler ultrasound blood flow velocity measurements were performed in 36 angiographically normal bifurcations. In these bifurcations the peak velocity over 2 cardiac cycles was measured and averaged in the mother branch M, the largest daughter branch D1 and the smaller daughter branch D2. The corresponding cross-sectional areas were determined by 3D analysis of biplane angiography (Guggenheim et al., 1991). From this data the flow and diameter for each branch was calculated assuming a parabolic flow profile and circular vessel area. Angiography was selected to determine the diameter since it allowed simultaneous recording of flow and diameter. The 18 bifurcations with the best imaging quality and flow measurements (the sum of the flow through the daughter branches was not allowed to deviate more than 10% from the flow through the mother branch) were selected for the analysis to determine two relationships. One fit was performed to obtain the relation between diameter and flow and a second fit to obtain the relation between the diameter ratio of the daughter branches and the flow ratio through these branches. The flow q (m³/s) and diameter d (m) of the 54 (18 times 3) branches was fitted to the equation
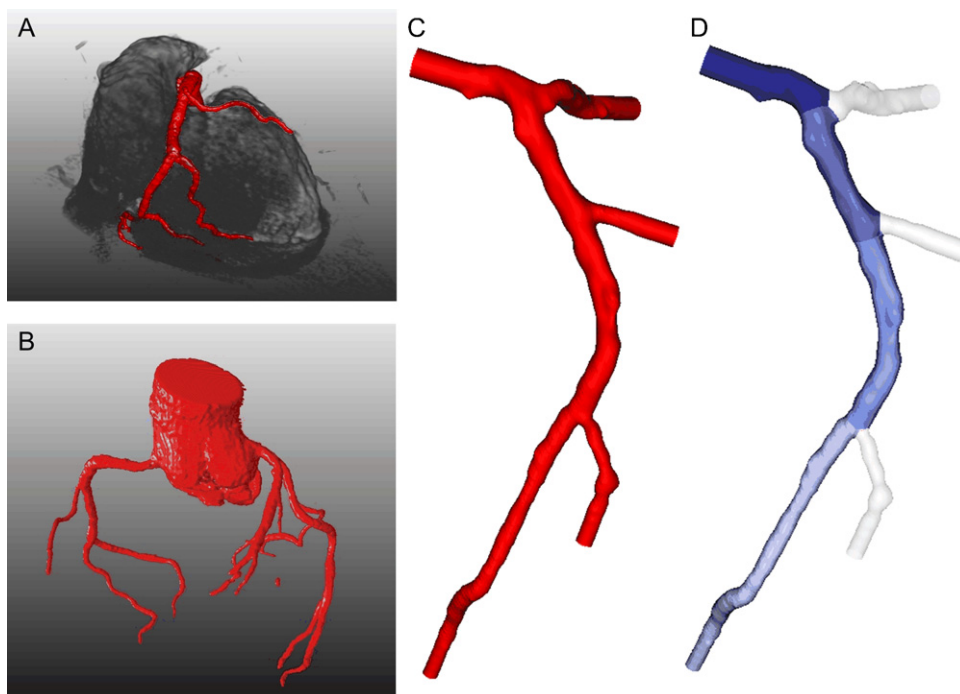
$$q = kd^x \tag{2}$$

Fig. 1. In panel A the segmentation of the coronary arteries is shown in the original MSCT scan. The complete segmented tree can be seen in panel B. This geometry is clipped, panel C, and the in- and outflow tracts are extended with circular tubes to aid the WSS computations. The geometry is divided in segments, panel D.

by non-linear regression analysis (Matlab 7.1, The MathWorks Inc.), with k (m²/s) as constant and the x (–) as power term. The relation between the flow ratio and the diameter ratio of the 18 bifurcations was fitted as

$$\frac{q_{D2}}{q_{D1}} = \left(\frac{d_{D2}}{d_{D1}}\right)^x \tag{3}$$

with the x (–) as power term. This relation will be referred to as Doriot's fit.

For both regressions the R^2 was determined and the 95% confidence interval (CI) of the estimated parameters.

2.2. WSS computations in patient specific coronary bifurcations

2.2.1. Image acquisition and analysis

We retrospectively selected coronary MSCT angiography datasets of patients that were scanned with a 64-slice MSCT scanner (Sensation64®, Siemens, Germany) in our institution. The reported spatial resolution of the resulting MSCT data set was $0.33 \times 0.33 \times 0.40$ mm³. A detailed description of the patient preparation, scan protocol and image reconstruction has previously been described (Mollet et al., 2005). We selected 10 coronary datasets that were judged as good quality MSCT scans (i.e. no moving artifacts, good contrast enhancement) by an experienced radiologist. The lumen of the coronary tree was segmented with dedicated MSCT image processing software (Leonardo, Siemens, Germany). The segmentation was based on intensity thresholds resulting in a binary voxel-space (see Fig. 1A and B). Although the segmentation software was not validated yet, the data represent patient specific 3D lumen data which is the main requirement for demonstrating the effect of different outflow models. We selected the three best segmented right coronary artery trees and three left anterior descending coronary artery trees, based on the completeness of the main artery and side branches. The selected arteries were angiographically normal with no significant stenosis. This implies that the reduction of the luminal cross sectional area was less than 50%, and therefore an interventional procedure was not justified. These binary coronary trees were converted into a surface and smoothed with the aid of imaging processing software (Mevislab, Mevis, Bremen, Germany). The surfaces were exported to the Vascular Modeling Toolkit (www.vmtk.org) to prepare the geometries for CFD. The coronary tree geometries were clipped at the side-branches such that the main artery and a short part of the side-branches remained to reduce computational cost. To allow prescription of in and outflow conditions, the inflow tract and all outflow tracts were extended with circular tubes in the direction of the centerline (Fig. 1C). Subsequently the coronary tree geometry was divided into segments (see Fig. 1D) (Antiga and Steinman, 2004) and the average diameter of each segment and side-branch was calculated.

2.2.2. Computational fluid dynamics

A volume mesh was created from the geometries with the mesh generator Gambit 2.4.6 (Ansys, Inc., USA) and discretized into linear tetrahedral volume elements. The elements had a maximum edge size of 0.2 mm at the model surface. For the CFD computations the blood was modeled as an incompressible non-Newtonian fluid with a density of 1050 kg/m³ using the Carreau model to describe the shear rate dependent viscosity of blood (Seo et al., 2005). The arterial wall was assumed to be rigid and with no-slip conditions at the wall. At the inlet and all outlet except for 1, a parabolic velocity profile was prescribed. At the remaining, most distal, outflow tract, a traction free boundary condition was applied. Both the inflow and outflow models were discussed in more detail in the next paragraph. A mesh refinement study was performed to ensure that the obtained solution was mesh independent. The solution was considered converged when the relative error in both the pressure and the velocities in all directions were lower than 10^{-3}.

2.2.3. Inflow and outflow conditions

We used the empirical relationship given in Eq. (2) to determine the inflow for our computational models. The average diameter of the inflow segment was determined for each model and the inflow was obtained by substituting the average diameter into Eq. (2). Two different models were applied to determine the flow ratio through the daughter branches: (1) Murray's Law (Eq. 1) and (2) Doriot's fit, the experimental derived flow–diameter ratio (Eq. (3)). The averaged diameters of the two daughter branches at each bifurcation serve as input for these equations. Once the flow ratio was known, the flow through the side-branch could be calculated and prescribed to the outflow tract using a parabolic velocity profile. For each geometry two WSS distributions were obtained: one derived using Murray's Law (WSS$_M$) and one derived using Doriot's fit as outflow condition model (WSS$_D$).

2.3. Data analysis

For the analysis different regions in the main branch were identified (see Fig. 2). For each side branch we defined the bifurcation region as that part of the main branch extending from 1 diameter upstream to one diameter
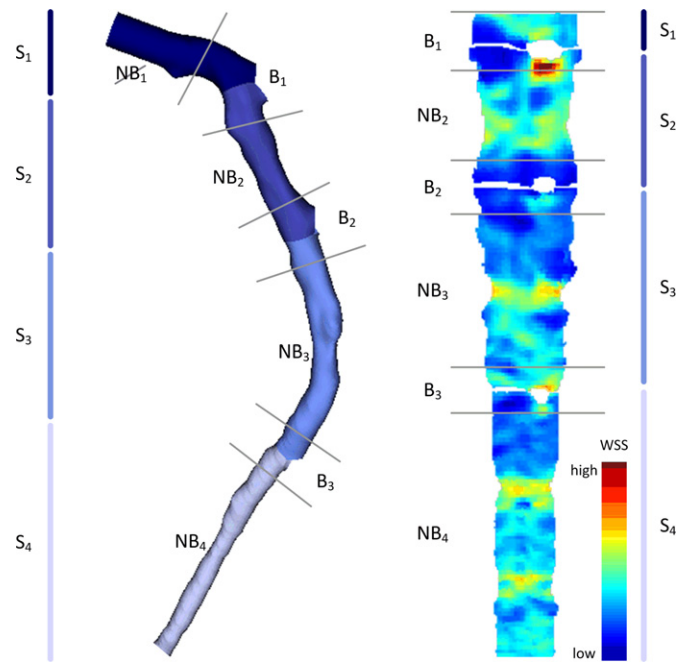

Fig. 2. Left: for the analysis of the WSS the side-branches are removed from the geometry. Besides the segments (S), bifurcation regions (B) and non-bifurcation regions (NB) are defined. The inflow segment is labeled as S1. Right: the same regions are now depicted in the 2D WSS map of the same artery.

downstream of the side branch. The remaining parts of the main branch were labeled as non-bifurcation regions. The relative difference between the WSS distributions was defined as (WSS$_M$−WSS$_D$)/WSS$_M$. For the bifurcation regions, we compared the size of the regions exposed to low WSS. The threshold for the low WSS region was determined for each artery separately and was equal to half the average WSS in the artery.

3. Results

3.1. Flow–diameter relation

Based on the data provided by Doriot et al. (2000) we derived two relations; between the diameter of the coronary branch and the flow through it (Eq. (2)) and between the diameter ratio of two daughter branches and the flow ratio through the branches (Eq. (3)).

The relation between flow and diameter (Eq. (2)) fitted very well ($R^2 = 0.87$), with the constants k of 1.43 m²/s (95% CI: −0.81–3.69 m²/s) and the power term x of 2.55 (95% CI: 2.27–2.83) resulting in Eq. (4). Fig. 3A shows this relation and the measured data.

$$q = 1.43d^{2.55} \tag{4}$$

The results of the non-linear regression for flow ratio and diameter ratio (Eq. (3)) are depicted in Fig. 3B. The power term x was 2.27 (95% CI: 1.58–2.96) resulting in Eq. (5)

$$\frac{q_{D2}}{q_{D1}} = \left(\frac{d_{D2}}{d_{D1}}\right)^{2.27} \tag{5}$$

The data were fitted with an R^2 of 0.70.

3.2. WSS computations

The geometries of the 6 patient derived coronary arteries are depicted in Fig. 4. The averaged diameters and prescribed flow through the segments and side branches are summarized in Table 1. As can be expected based on the results of Eq. (5), the
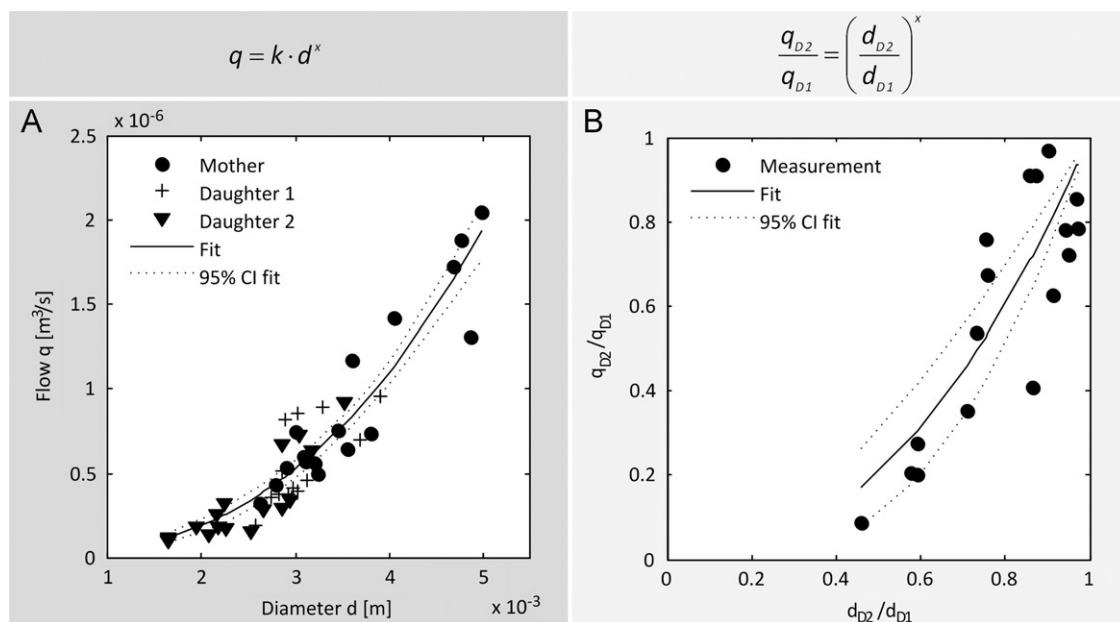
$$q = k \cdot d^x$$

$$\frac{q_{D2}}{q_{D1}} = \left(\frac{d_{D2}}{d_{D1}}\right)^x$$

Fig. 3. Results of the fitting procedures on data of Doriot et al. (2000). On the left (panel A) the relation between the flow and the diameter of the artery is fitted (Eq. (4)). On the right (panel B) the relation between the flow ratio and diameter ratio of the smaller daughter branch D2 and larger daughter branch D1 is fitted as described by Eq. (5).
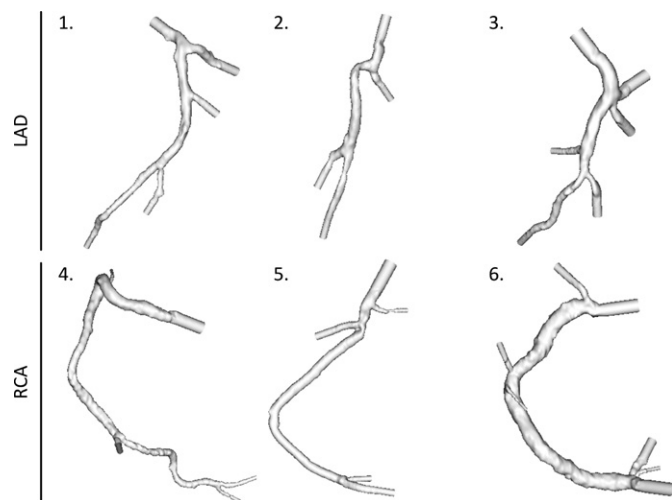

Fig. 4. The geometries in which the WSS for different outflow condition models are computed. Geometries 1–3 are left descending coronary arteries and 4–6 are right coronary arteries.

Table 1
Geometry characteristics and boundary conditions.

Geometry	Bifurcation	Diameter (mm)			Flow (ml/min)			
					Murray's Law		Doriot's fit	
		M	D1	D2	M	D2	M	D2
1	1	3.45	3.77	3.30	<u>45.0</u>	<u>18.0</u>	<u>45.0</u>	<u>19.1</u>
	2	3.77	3.32	2.59	27.0	<u>8.7</u>	25.9	<u>9.4</u>
	3	3.32	2.37	2.09	18.3	<u>7.5</u>	16.5	<u>7.1</u>
2	1	2.81	2.83	2.11	<u>26.7</u>	<u>7.8</u>	<u>26.7</u>	<u>9.0</u>
	2	2.83	2.09	2.03	18.9	<u>9.1</u>	17.7	<u>8.6</u>
3	1	4.73	5.07	3.53	<u>101.0</u>	<u>25.4</u>	<u>101.0</u>	<u>30.8</u>
	1a	5.07	3.58	3.13	75.6	<u>30.2</u>	70.2	<u>29.7</u>
	2	3.58	2.44	2.36	45.4	<u>21.5</u>	40.5	<u>19.4</u>
	3	2.44	2.44	2.36	23.8	<u>11.3</u>	21.0	<u>10.1</u>
4	1	5.20	3.98	1.30	<u>128.5</u>	<u>4.3</u>	<u>128.5</u>	<u>9.3</u>
	2	3.98	2.90	2.50	124.2	<u>48.3</u>	119.2	<u>49.5</u>
	3	2.90	1.86	1.56	75.9	<u>28.1</u>	41.8	<u>27.9</u>
5	1	4.72	3.68	1.87	<u>100.4</u>	<u>11.6</u>	<u>100.4</u>	<u>17.7</u>
	2	3.68	3.37	2.58	88.8	<u>27.5</u>	82.7	<u>29.1</u>
	3	3.37	2.49	1.97	61.3	<u>20.3</u>	53.5	<u>19.8</u>
6	1	4.77	5.45	2.56	<u>103.4</u>	<u>9.7</u>	<u>103.4</u>	<u>15.7</u>
	2	5.45	4.85	2.52	93.8	<u>11.5</u>	87.7	<u>16.2</u>
	3	4.85	5.19	1.84	82.2	<u>3.5</u>	71.5	<u>6.2</u>
	4	5.19	4.67	3.35	78.7	<u>21.2</u>	65.3	<u>20.9</u>
	5	4.67	4.52	1.66	57.5	<u>2.7</u>	44.4	<u>4.1</u>

M is the mother branch; D1 is daughter branch 1; D2 is daughter branch 2, daughter 2 is always the smaller daughter branch; the prescribed flow in the CFD computations are underlined; geometry 3, bifurcation 1a is part of a trifurcation, for the analysis it is treated as 1 bifurcation region together with bifurcation 1.

total flow through the side-branches was higher when prescribing outflow conditions according to Doriot's fit versus Murray's law, resulting in lower flow through the main branch.

An example (LAD, geometry 1) of WSS_M is shown in Fig. 5A. The first side branch is the left circumflex artery, which has a large diameter. As a consequence, a low WSS region is present opposite of the flow divider. Further downstream, local lumen narrowing results in increased WSS_M values. Since this is a relatively straight segment, no pronounced effect of curvature is observed. The WSS_M slightly increases going from proximal to distal. The average WSS_M was 0.26 Pa (95% CI: 0.08–0.51 Pa) with a maximum of 1.02 Pa immediately downstream of the most proximal bifurcation. Fig. 5B depicts the WSS_D and Fig. 5C the relative difference between Murray's law and Doriot's fit. The relative difference between the two models ranged from −14.4% to 17.1% and is most pronounced near the bifurcation regions.

In non-bifurcation regions, the relative difference is fairly constant. Application of Murray's Law results in higher flow rates through the main branch, and we therefore expect WSS_M to exceed WSS_D in non-bifurcation regions. If we study the average relative difference in WSS along the length of the artery, we can see that this averaged relative difference scales with the relative difference in flow rate (Fig. 5D).

For all the 6 coronary arteries, the averaged relative difference between WSS_M and WSS_D in the non-bifurcation regions can be fairly large and ranges from −5.1% to 27.4%. For Murray's Law,
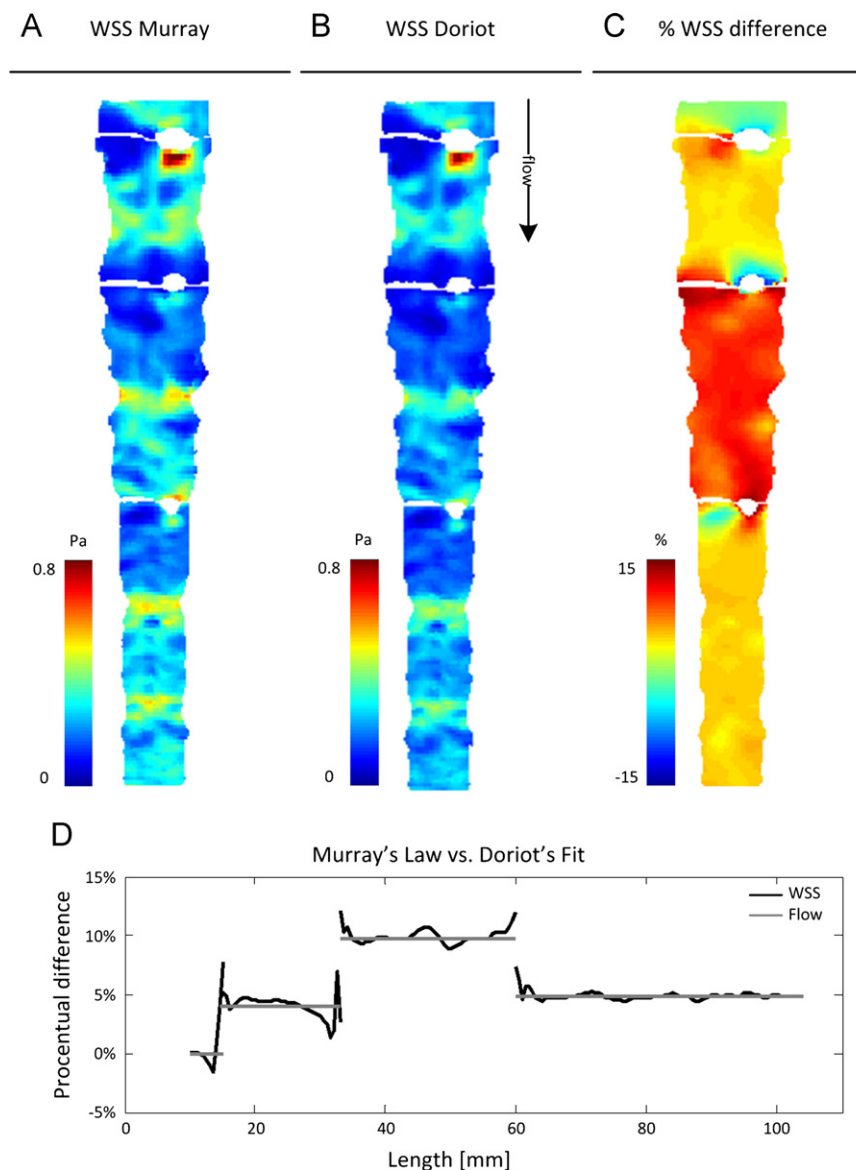
Fig. 5. Panel A shows the WSS_M mapped into 2D. In panel B the WSS_D and panel C the relative difference between the WSS_M and WSS_D is depicted. It shows that the relative difference is fairly constant outside of the bifurcation regions. In panel D the relative difference in WSS is averaged over the circumference and plotted against the length of the artery, and it demonstrates that the relative difference in WSS is close to the relative difference in flow through the branch.

flow through the main branch is generally larger, and the average WSS in the non-bifurcation regions is therefore higher (8.3 ± 7.7, $p < 0.05$). For all the non-bifurcation regions, these differences scale with the difference in flow. Linear regression supported that the relative differences in flow and WSS in the non-bifurcation regions were equal ($R^2 = 0.96$, slope$= 1.08$ and offset$= 0.01$).

For the bifurcation regions, the differences between the WSS patterns for the two outflow models are more pronounced. The shape and the size of the low WSS region depends on the differences in flow rate and local geometric features, and low WSS region can be either larger or smaller when comparing Murray's Law to Doriot's fit (Fig. 6). For all the bifurcation regions studied, the larger low WSS region always overlapped the smaller one. Generally speaking, since flow through the side branches is larger when applying Doriot's fit, the low WSS region for that model is larger ($13.1 \pm 6.2\%$, $p < 0.05$). For all the bifurcation regions, the observed differences in the size of the low WSS area between Doriot's fit and Murray's Law vary from -12% to $+68\%$.

4. Discussion

MSCT is a promising non-invasive imaging technique that can provide geometrical data of the coronary arteries to compute WSS in the complete arterial tree, including the bifurcation regions. MSCT angiography does not provide hemodynamic information that is necessary to prescribe the in- and outflow boundary conditions. In this study we provide diameter-based models to determine these boundary conditions. The inflow for the artery was estimated based on a relationship that was derived from the measured flow and diameter data of Doriot et al. (2000). To estimate the outflow for the side-branches Murray's Law is commonly used, which states that the flow division over two branches equals the ratio of the diameters to the power 3. In literature, lower values are found (VanBavel and Spaan, 1992; Mittal et al., 2005) and our study confirms this: the fitting procedure resulted in a value of 2.27. We studied the effect of different outflow conditions on the WSS distribution and showed that in the non-bifurcation regions, application of Murray's Law
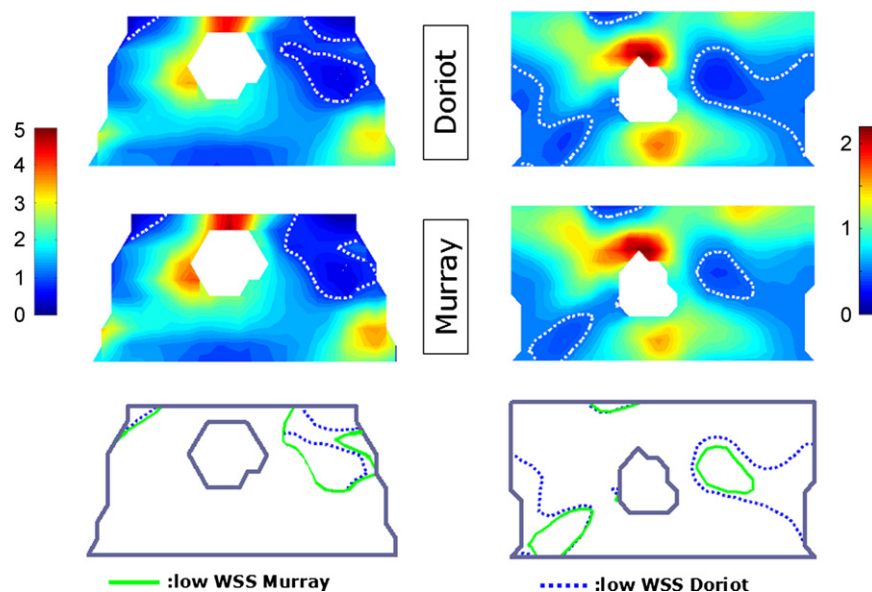
Fig. 6. Two examples of the WSS distribution in bifurcation regions. The top panels show the WSS distribution for Doriot's fit, the central panels for Murray's model, and the bottom two panels show the low WSS regions for the two panels. The left column illustrates an example in which the low WSS region is larger when applying Murray's law, and the right column shows a bifurcation region for which the low WSS region is larger when applying Doriot's fit.

significantly overestimates average WSS values compared to Doriot's fit and that these differences scale with the prescribed flow through the branch. In the bifurcation regions, application of Murray's law underestimates the size of the low WSS regions significantly when compared to Doriot's fit.

The mean WSS in our study is 0.68 Pa, which is lower than the values that are generally used in studies in which no flow data were available (1.4–17.7 Pa (Gijsen et al., 2007; Soulis et al., 2006; Saihara et al., 2006; Wentzel et al., 2005)). However, the mean WSS value from this study is within the range of studies that determined WSS based on measured flow data (0.46–1.24 Pa (Gijsen et al., 2003, 2008)). Therefore it seems to be appropriate to use our proposed diameter–flow relationships in studies where patient specific flow data is not available.

Murray's Law is most often applied to determine the flow ratio over the side branches (Gijsen et al., 2007; Soulis et al., 2006; Joshi et al., 2004). However, reports on the diameter distribution of coronary arterial trees find a lower power value than the third power of Murray's Law (VanBavel and Spaan, 1992; Finet et al., 2008). To our knowledge we are the first that determined in human coronary arteries the relation between the diameter ratio and the flow ratio of the daughter branches. We found also a lower power value of 2.27. Since both literature based on diameter and our data come up with a lower power value, it seems to be more appropriate to prescribe higher flow rates through the side-branches than those derived from Murray's Law. This will result in lower flows through the main branch, and thus lower Reynolds numbers. As a consequence, the size of the low WSS regions in bifurcation regions is significantly affected. How the differences between the two models influence findings on the relationship between WSS and pathological parameters like local wall thickening requires more in vivo clinical studies.

4.1. Limitations

When studying atherosclerosis in the coronary arteries a wide variety of disease can be present, from early atherosclerosis with no flow limiting plaque to the more advanced phases of the disease with highly stenotic plaques. The data we used for the fitting of the flow–diameter relations was obtained in patients with coronary artery disease, but in angiographically normal segments. The boundary condition models we presented in this paper might thus not be applicable for more diseased arteries. More volumetric flow measurements in different patients groups will improve the proposed models and extend applicability of the model to more advanced atherosclerotic coronary trees. Unfortunately, when intravascular Doppler measurements are performed, only maximum velocity is reported without the corresponding diameter at the measured location. Instead of Doppler measurements, for future research other measuring techniques might be more appropriate (Lupotti et al., 2003), since they can provide both coronary size and flow rate without necessary assumptions regarding the velocity profile. Furthermore, to convert the Doppler velocity measurements to flow rates, we used the lumen cross sectional area derived from biplane angiography. Invasive imaging techniques would potentially improve the estimation of lumen cross sectional area. However, in a recent publication (Schuurbiers et al., 2008) we demonstrated a good agreement between in vivo lumen area derived from IVUS and biplane angiography in human coronary arteries.

In this study, we used experimental data to determine the relationship between flow through the side branch and its diameter. Other studies used mathematical models to generate the coronary vascular tree to determine resistance of and flow through the side branch (VanBavel and Spaan, 1992; Huo and Kassab, 2007; Molloi and Wong, 2007; Kaimovitz et al., 2005). Lumped parameters models can be used to represent the vascular bed, and recently these were combined with 3D models of the aorta to determine the flow through outflow tracts (Mittal et al., 2005; Huo and Kassab, 2007; Olufsen, 1999). In the coronary arteries however not only the properties of the distal vascular bed, but also the contraction of the heart muscle will influence the flow. More complex models are developed that model the coronary flow (Bovendeerd et al., 2006), but these are not yet coupled to 3D models for CFD computations. All these models with increasing complexities have great potential to mimic flow and thus WSS in the coronary arteries with increasing physiological resemblance. However, patient specific measurements at several locations in the coronary arteries and in different stages of

disease will be necessary to determine the parameters in such models.

Besides increasing complexity in prescribing boundary conditions also the complexity of the 3D model can be increased. In this study we choose for a simple static, rigid 3D model of the coronary arteries in which we computed time-averaged WSS. Several papers have investigated the effect of these simplifications in a numerical way (Ramaswamy et al., 2004; Pivkin et al., 2005; Prosi et al., 2004; Zeng et al., 2008). These studies show that simplifications of the 3D model have some influence on the WSS values. However, how these simplifications will influence the findings on the relationship between WSS and atherosclerosis is unknown, since in most clinical studies that relate WSS to atherosclerosis, the WSS values are normalized or averaged in the spatial domain.

We used MSCT in this study to derive patient specific lumen information. Although the reported resolution of MSCT is good, the resulting images contain artifacts due to blooming of the contrast and the presence of calcium (Olufsen, 1999). This implies that validation of MSCT as a stand-alone imaging modality for computational applications to study the relationship between atherosclerosis and WSS is required.

Finally, numerical investigations like the one presented in this study generally benefit from experimental validation. The simulations reveal rather subtle differences between the WSS distribution derived from Murray's Law and the ones obtained from Doriot's fit. Confirmation of these results from experimental studies would further strengthen the conclusions reached in this study.

5. Conclusion

When lacking patient specific boundary conditions for WSS computations in coronary trees, an estimation of the flow rates is necessary. Pending further validation, we propose an empirical relationship—Doriot's fit—that relates the local geometry to flow rates through the main and side-branches. When applied as a boundary condition, Doriot's fit results in lower average WSS in the main branch and larger low WSS regions near bifurcations when compared to the commonly applied Murray's Law.

Conflict of interest statement

None declared.

References

Antiga, L., Steinman, D.A., 2004. Robust and objective decomposition and mapping of bifurcating vessels. IEEE Trans. Med. Imaging 23 (6), 704–713.

Boutsianis, E., et al., 2004. Computational simulation of intracoronary flow based on real coronary geometry. Eur. J. Cardiothorac. Surg. 26 (2), 248–256.

Bovendeerd, P.H., et al., 2006. Dependence of intramyocardial pressure and coronary flow on ventricular loading and contractility: a model study. Ann. Biomed. Eng. 34 (12), 1833–1845.

Chatzizisis, Y.S., et al., 2008. Prediction of the localization of high-risk coronary atherosclerotic plaques on the basis of low endothelial shear stress: an intravascular ultrasound and histopathology natural history study. Circulation 117 (8), 993–1002.

Cunningham, K.S., Gotlieb, A.I., 2005. The role of shear stress in the pathogenesis of atherosclerosis. Lab. Invest. 85 (1), 9–23.

Doriot, P.A., et al., 2000. In-vivo measurements of wall shear stress in human coronary arteries. Coron. Artery Dis. 11 (6), 495–502.

Finet, G., et al., 2008. Fractal geometry of arterial coronary bifurcations: a quantitative coronary angiography and intravascular ultrasound analysis. EuroIntervention 3 (4), 490–498.

Frauenfelder, T., et al., 2007. In-vivo flow simulation in coronary arteries based on computed tomography datasets: feasibility and initial results. Eur. Radiol. 17 (5), 1291–1300.

Gijsen, F.J., et al., 2003. Usefulness of shear stress pattern in predicting neointima distribution in sirolimus-eluting stents in coronary arteries. Am. J. Cardiol. 92 (11), 1325–1328.

Gijsen, F.J., et al., 2007. A new imaging technique to study 3-D plaque and shear stress distribution in human coronary artery bifurcations in vivo. J. Biomech. 40 (11), 2349–2357.

Gijsen, F.J., et al., 2008. Strain distribution over plaques in human coronary arteries relates to shear stress. Am. J. Physiol. Heart Circ. Physiol. 295 (4), H1608–H1614.

Guggenheim, N., et al., 1991. Spatial reconstruction of coronary-arteries from angiographic images. Phys. Med. Biol. 36 (1), 99–110.

He, X., Ku, D.N., 1996. Pulsatile flow in the human left coronary artery bifurcation: average conditions. J. Biomech. Eng. 118 (1), 74–82.

Huo, Y., Kassab, G.S., 2007. A hybrid one-dimensional/Womersley model of pulsatile blood flow in the entire coronary arterial tree. Am. J. Physiol. Heart Circ. Physiol. 292 (6), H2623–H2633.

Jeremias, A., et al., 2000. Spatial orientation of atherosclerotic plaque in non-branching coronary artery segments. Atherosclerosis 152 (1), 209–215.

Joshi, A.K., et al., 2004. Intimal thickness is not associated with wall shear stress patterns in the human right coronary artery. Arterioscler. Thromb. Vasc. Biol. 24 (12), 2408–2413.

Kaimovitz, B., Lanir, Y., Kassab, G.S., 2005. Large-scale 3-D geometric reconstruction of the porcine coronary arterial vasculature based on detailed anatomical data. Ann. Biomed. Eng. 33 (11), 1517–1535.

Krams, R., et al., 1997. Evaluation of endothelial shear stress and 3D geometry as factors determining the development of atherosclerosis and remodeling in human coronary arteries in vivo. Combining 3D reconstruction from angiography and IVUS (ANGUS) with computational fluid dynamics. Arterioscler. Thromb. Vasc. Biol. 17 (10), 2061–2065.

LaBarbera, M., 1990. Principles of design of fluid transport systems in zoology. Science 249 (4972), 992–1000.

Lupotti, F.A., et al., 2003. Quantitative IVUS blood flow: validation in vitro, in animals and in patients. Ultrasound Med. Biol. 29 (4), 507–515.

Malek, A.M., Alper, S.L., Izumo, S., 1999. Hemodynamic shear stress and its role in atherosclerosis. J. Am. Med. Assoc. 282 (21), 2035–2042.

Mittal, N., et al., 2005. Analysis of blood flow in the entire coronary arterial tree. Am. J. Physiol. Heart Circ. Physiol. 289 (1), H439–H446.

Mollet, N.R., et al., 2005. High-resolution spiral computed tomography coronary angiography in patients referred for diagnostic conventional coronary angiography. Circulation 112 (15), 2318–2323.

Molloi, S., Wong, J.T., 2007. Regional blood flow analysis and its relationship with arterial branch lengths and lumen volume in the coronary arterial tree. Phys. Med. Biol. 52 (5), 1495–1503.

Olufsen, M.S., 1999. Structured tree outflow condition for blood flow in larger systemic arteries. Am. J. Physiol. 276 (1 Pt 2), H257–H268.

Perktold, K., Nerem, R.M., Peter, R.O., 1991. A numerical calculation of flow in a curved tube model of the left main coronary artery. J. Biomech. 24 (3–4), 175–189.

Pivkin, I.V., et al., 2005. Combined effects of pulsatile flow and dynamic curvature on wall shear stress in a coronary Artery bifurcation model. J. Biomech. 38, 1283–1290.

Prosi, M., et al., 2004. Influence of curvature dynamics on pulsatile coronary artery flow in a realistic bifurcation model. J. Biomech. 37 (11), 1767–1775.

Ramaswamy, S.D., et al., 2004. Fluid dynamic analysis in a human left anterior descending coronary artery with arterial motion. Ann. Biomed. Eng. 32 (12), 1628–1641.

Saihara, K., et al., 2006. Association of coronary shear stress with endothelial function and vascular remodeling in patients with normal or mildly diseased coronary arteries. Coron. Artery Dis. 17 (5), 401–407.

Schuurbiers, J.C., Lopez, N.G., Ligthart, J., Gijsen, F.J., Dijkstra, J., Serruys, P.W., Van der Steen, A.F., Wentzel, J.J., 2008. In vivo validation of CAAS QCA-3D coronary reconstruction using fusion of angiography and intravascular ultrasound (ANGUS). Catheter Cardiovasc. Interv. 73, 620–626.

Seo, T., Schachter, L.G., Barakat, A.I., 2005. Computational study of fluid mechanical disturbance induced by endovascular stents. Ann. Biomed. Eng. 33 (4), 444–456.

Slager, C.J., et al., 2005. The role of shear stress in the generation of rupture-prone vulnerable plaques. Nat. Clin. Pract. Cardiovas. Med. 2 (8), 401–407.

Slager, C.J., et al., 2000. True 3-dimensional reconstruction of coronary arteries in patients by fusion of angiography and IVUS (ANGUS) and its quantitative validation. Circulation 102 (5), 511–516.

Soulis, J.V., et al., 2006. Wall shear stress in normal left coronary artery tree. J. Biomech. 39 (4), 742–749.

VanBavel, E., Spaan, J.A., 1992. Branching patterns in the porcine coronary arterial tree. Estimation of flow heterogeneity. Circ. Res. 71 (5), 1200–1212.

Wentzel, J.J., et al., 2003. Extension of increased atherosclerotic wall thickness into high shear stress regions is associated with loss of compensatory remodeling. Circulation 108 (1), 17–23.

Wentzel, J.J., et al., 2005. Geometry guided data averaging enables the interpretation of shear stress related plaque development in human coronary arteries. J. Biomech. 38 (7), 1551–1555.

Zeng, D., et al., 2008. A study on the compliance of a right coronary artery and its impact on wall shear stress. J. Biomech. Eng. 130 (4), 041014.